Chapter 5 16 October 1999 M=7.1 Hector Mine, California, earthquake

The 1999 M_w7.1 Hector Mine earthquake sequence was the most recent of a series of moderate to large earthquakes on the Eastern California Shear Zone, which include the 1947 M 6.5 Manix, 1992 M_w 6.1 Joshua Tree, and M_w 7.3 Landers sequences (Hauksson et al., 2002). The mainshock was preceded by a cluster of 18 $1.5 \leq M \leq 3.8$ foreshocks within 1 km of the mainshock hypocenter, located at 34.59°N and 116.27°W at a depth of 5 km (Hauksson et al., 2002). It was well recorded by stations of the Southern California Seismic Network (SCSN)- the Southern California portion of the California Integrated Seismic Network (CISN), with station Hector (HEC) being the closest at about 27 km north of the hypocenter (10.7 km closest distance to the fault) (Grazier et al., 2002).

5.1 Road map

The Virtual Seismologist (VS) method for seismic early warning is applied to the Hector Mine mainshock dataset, using seismograms from high dynamic range, real-time telemetered SCSN stations. Following a few comments on station geometry in the Eastern Mojave, the VS single station estimates for magnitude and epicentral distance based on the data available 3 seconds after the initial P detection at the first station are presented. As would be expected, these data (3-sec amplitudes at a single station) are not enough to uniquely constrain the magnitude and location. A Bayesian approach resolves these trade-offs in favor of prior information. What is included in the Bayes prior affects the initial VS estimates. These effects are illustrated.

The initial VS estimate is updated as the ground motions propagate to further stations. The updated VS estimates at 5.5, 7, 8, 14, 34, and 74 seconds after the

initial P detection are discussed. These updated VS estimates are expressed in terms of magnitude and epicentral location (as opposed to epicentral distance). Working with epicentral location allows information regarding previously observed seismicity and possibly fault locations to be included in the Bayes prior. The foreshock sequence of 18 spatially clustered events in the 24 hours preceding the Hector Mine mainshock provides very strong prior information.

Aside from P-arrivals and observed amplitudes, at any given time, the lack of arrivals at adjacent stations is a valuable constraint. The use of not-yet arrived data builds upon recent work of Rydelek and Pujol (2004) and Horiuchi et al. (2004). The constraint from non-arrivals is particularly important for regions where the distance between stations, and hence the time between arrivals, is relatively large. For the Hector Mine event, the interval between the first two arrivals is nearly 8 seconds. The evolution of possible locations as a function of both arrivals and non-arrivals will be presented. Note that the use of not-yet arrived data in the VS method differs from Rydelek and Pujol (2004) and Horiuchi et al. (2004) in that this information is used to constrain locations immediately following the first P detection.

The first few VS estimates the more important for seismic early warning. However, the VS estimates for large times after the origin or initial P detection can be used as robust amplitude-based checks on the arrival-based locations typically determined by the seismic network. The amplitude-based location estimates (VS location estimate using a uniform prior and not including any arrival information) from the Hector Mine ground motions are discussed. Such amplitude-based locations are comparable to the strong motion centroid of Kanamori (1993).

Finally, the observed peak P- and S-wave amplitudes from the Hector Mine mainshock are compared to the expected levels ground motion levels from the envelope attenuation relationships developed in Chapter 2. (There should be fairly good agreement between the expected and observed values, since the Hector Mine dataset was among the events used to obtain the envelope attenuation relationships.)

5.2 SCSN stations in the epicentral region

A snapshot of the operating SCSN station (within 250 km of the epicenter) at the time of the M=7.1 Hector Mine mainshock is shown in Figure 5.1. (These are actually stations that recorded ground motions from the mainshock. It is assumed that if a particular station recorded data, then it was operating before the mainshock.) The polygons define the nearest neighbor regions of the stations (triangles) about which they are centered. If station A has the first P detection, then the earthquake is constrained to be located within station A's nearest neighbor region, or Voronoi cell. The shape of these Voronoi cells is a function of the locations of operational stations at any given time. They change whenever additional stations are put on-line or stations are taken off-line. Ideally, the Voronoi cells and their associated characteristics (areas and epicentral distances consistent with being within a station's Voronoi cell) should be updated whenever there is a change of operating status at any station of the seismic network. For the Hector Mine mainshock, the first triggered station is HEC (Hector), located about 27 km from the epicenter. HEC's Voronoi cell is shaded in Figure 5.1. The surface faulting (from Chen Ji, pers. comm.) is also shown. The Voronoi cells around the epicentral region have relatively large areas, due to the low density of SCSN stations with high dynamic range and real-time telemetry in this region. Table 5.1 lists the locations, Voronoi areas, epicentral distances, fault distances, and P wave arrival times at station HEC and the stations sharing a Voronoi edge with HEC. The Voronoi areas in the Hector Mine mainshock epicentral region are an order of magnitude larger than those in the epicentral region of the Yorba Linda mainshock (Table 8.1 in Chapter 8). The locations of $M \geq 1$ events located by SCSN in the 24 hours preceding the mainshock are marked by circles. There were 40 such events in the region from $32°N$ to $36°N$ and $120°W$ to $115°W$; 18 of these occurred within HEC's Voronoi cell, within 1 km epicentral distance of the mainshock epicenter (Hauksson et al., 2002).

Figure 5.2 shows the observed vertical acceleration records from HEC and the stations sharing a Voronoi edge with HEC. There is nearly 8 seconds between the

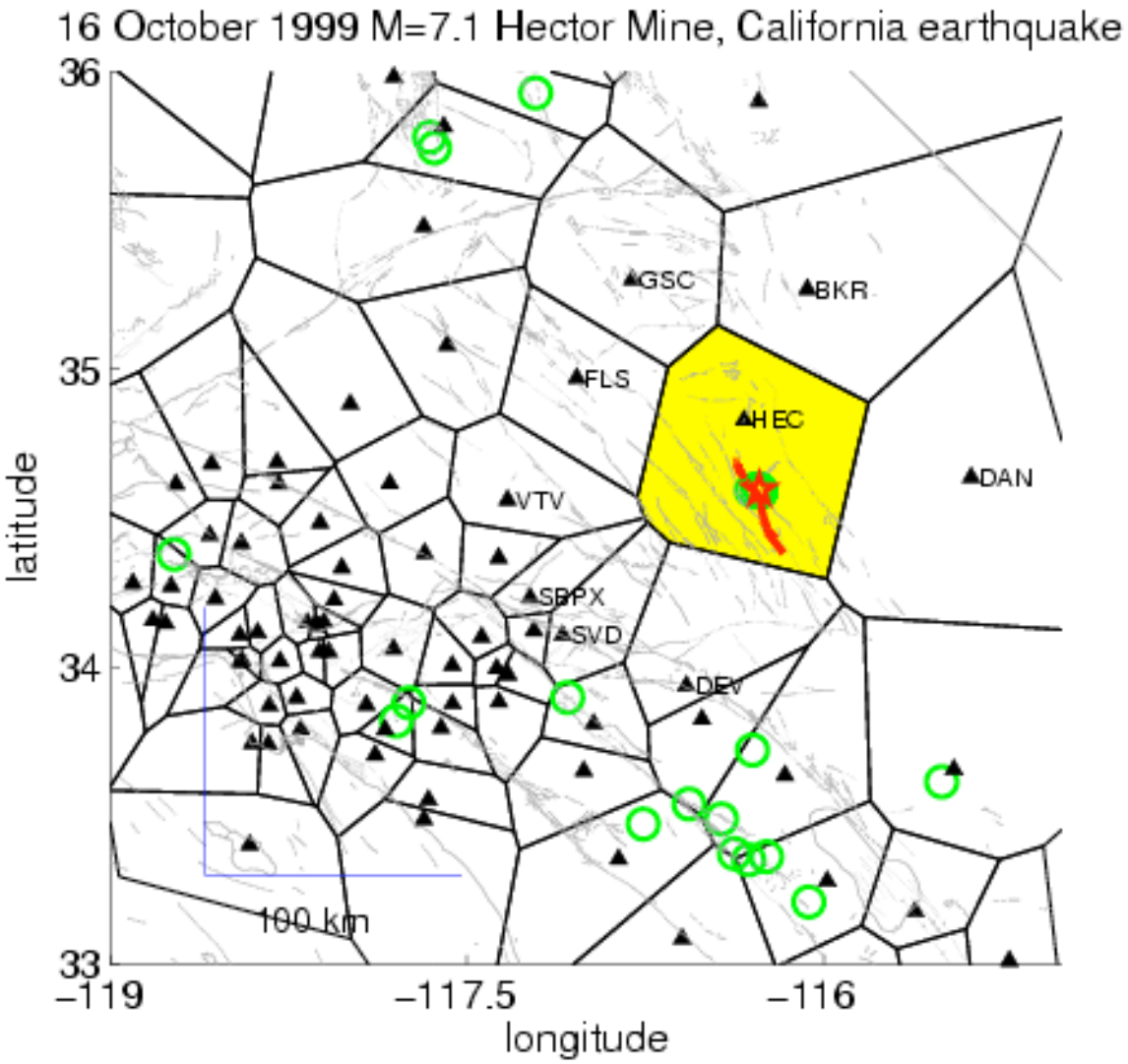

Figure 5.1: Map of SCSN stations that recorded ground motions from the 16 October 1999 $M = 7.1$ Hector Mine, California earthquake. Circles are locations of $M \geq 1$ earthquakes recorded by the Southern California Seismic Network (SCSN) in the 24 hours prior to the mainshock. 18 of the 40 earthquakes were located within 1 km epicentral distance of the mainshock hypocenter (Hauksson et al., 2002).

Stations closest to the $M = 7.1$ Hector Mine mainshock

Station name	Abrev	Lon	Lat	Vor. area km^2	Ep. dist. km	Fault dist. km	Arrv. sec
Hector	HEC	-116.335	34.829	5804	26.7	10.7	6.0
Baker	BKR	-116.070	35.269	8021	77.1	68.6	13.7
Devers	DEV	-116.578	33.936	3322	78.8	62	13.9
Danby	DAN	-115.381	34.637	9299	81.8	77.6	14.5
Flash2 Pk.	FLS	-117.039	34.970	2933	81.8	67.9	14.5
Goldstone	GSC	-116.806	35.302	4523	92.5	77.6	16.2
Seven Oaks Dam	SVD	-117.098	34.106	1513	93.4	88.2	16.3
Victorville	VTV	-117.330	34.561	2198	97.2	89.2	16.9
Strawberry Pk.	SBPX	-117.235	34.232	880	97.3	93.8	16.9

Table 5.1: Some stations within 100 km of the $M = 7.1$ Hector Mine mainshock. The SCSN station closest to the mainshock is Hector (HEC), 26.7 km from the epicenter and 14.4 km from the closest part of the Lavic Lake fault. The fault trace was obtained from Ji Chen (pers. comm.). The other stations listed share a Voronoi edge with HEC. The areas of the Voronoi cells in this region of the network are about an order of magnitude larger than those in the vicinity of the Yorba Linda mainshock (Table 8.1 in Chapter 5).

initial P detection at HEC and the second arrival at the second closest station, Baker (BKR). The vertical lines marked "T0" and "T1" are the theoretical P and S wave travel times using the SCSN location of $34.5940°N, 116.2710°W$.

5.3 Single station estimates: solving for magnitude and epicentral distance

With data from a single station, the VS method can be used to solve for either 1) magnitude and epicentral distance or 2) magnitude and epicentral location. The VS estimates for magnitude and epicentral distance using the first 3 seconds of data after the initial P detection at HEC are presented first.

Let Z.a, Z.v, and Z.d refer to the maximum vertical acceleration, velocity, and filtered displacement envelope amplitudes observed between the P detection at a station and some time t. (In the examples in this thesis, it is assumed that P-waves

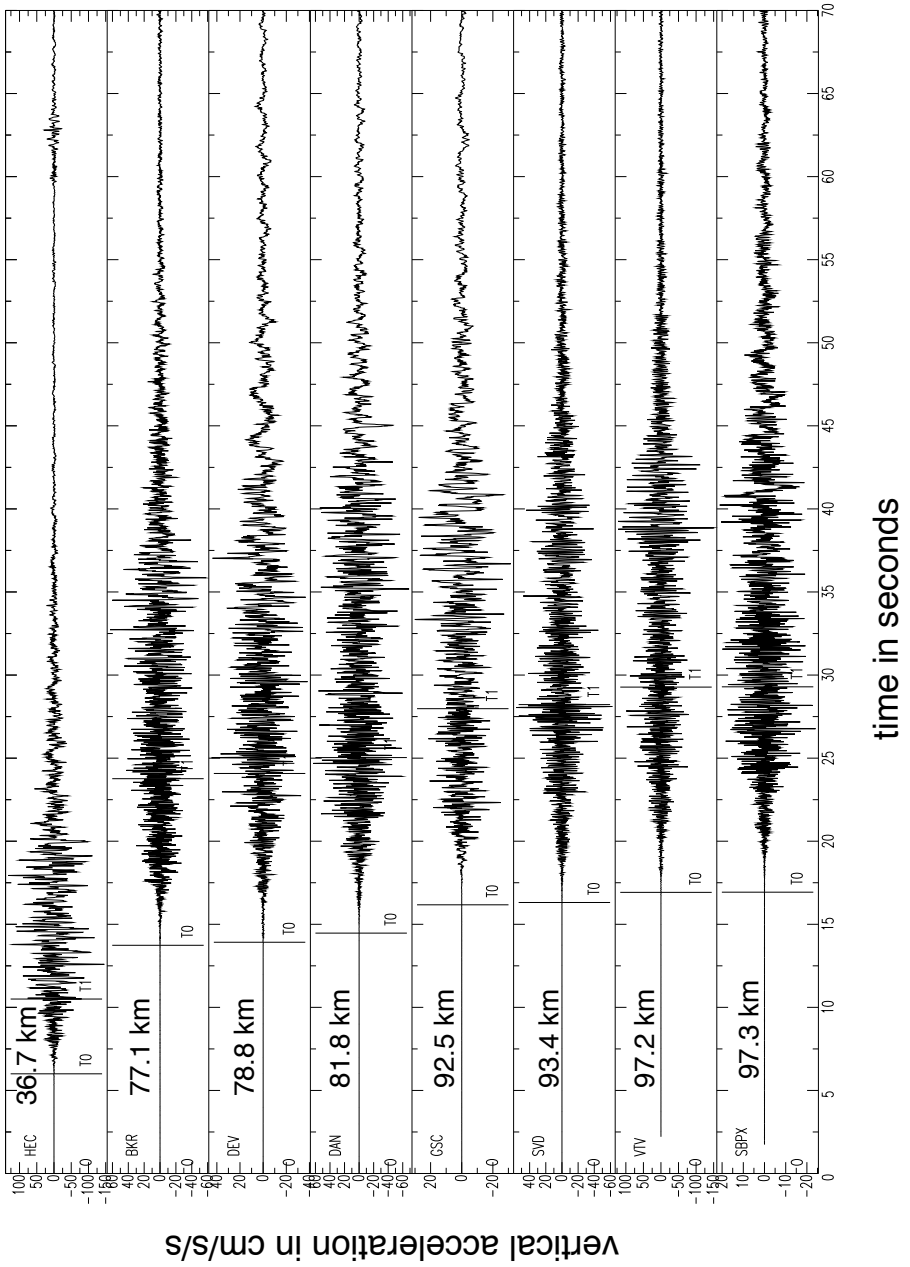

Figure 5.2: Vertical acceleration records from stations within 100 km of the Hector Mine mainshock. Vertical lines marked "T0" and "T1" are the P and S arrival times, respectively. Arrival times were calculated using Eaton's travel time code with a 1D, 6 layer Southern California velocity model (Hauksson, pers. comm.). Manual adjustments were made to the arrivals times when necessary. The distances listed are epicentral distances.

can be detected efficiently using short-term over long-term average methods.) EN.a, EN.v, and EN.d are the corresponding envelope amplitudes for the root mean square of the maximum amplitudes of the horizontal channels.

Figure 5.3 (a) shows the P/S discriminant function (discussed in Appendix C) as a function of time. The P/S discriminant function is $PS = 0.4\log_{10}(Z.a) + 0.55\log_{10}(Z.v) - 0.46\log_{10}(EN.a) - 0.55\log_{10}(EN.v)$. The first zero crossing of P/S after the P arrival indicates the S-wave arrival. The method expects the P-wave to be larger on the vertical and smaller on the horizontal, and the converse for the S-wave. As discussed in Appendix C, this discriminant has a misclassification error of 15%. It does not perform well for the ground motions at HEC since the vertical and horizontal P-wave envelopes are of comparable amplitude (Figure 5.4.) Figure 5.3 (b) shows ratio $Z_{ad} = Z.a^{0.36}/Z.d^{0.93} = 0.36\log_{10}(Z.a) - 0.93\log_{10}(Z.d)$ as a function of time. The left-hand axis shows the P-wave decision boundaries; those on the right, the S-wave decision boundaries. Misclassifying the P-wave amplitudes as S-waves leads initially leads to lower magnitude estimates.

There are certain ranges of Z_{ad} where the estimated magnitude range does not depend on whether the amplitudes are from P- or S-waves (Figure 5.3). For example, an observed ground motion ratio of $Z_{ad} = 1.73$ would be classified as belonging to the $5 \leq M \leq 6$ group, regardless of which set of decision boundaries (left hand side for P-waves, right hand side for S-waves) are used. However, an earthquake generating a ground motion ratio of $Z_{ad} = 1.70$ would most probably belong (with some chance of misclassification) to the $M \geq 6$ group if the amplitudes are assumed or determined to be from a P-wave, but to the $5 \leq M \leq 6$ group if the amplitudes were from an S-wave. If the 3-second amplitude observations for HEC are treated as S-wave amplitudes, as suggested by the P/S discriminant, the initial estimated magnitude range is $5 \leq M \leq 6$. As the actual S-wave amplitudes arrive, the estimate adjusts to $M \geq 6$. If the 3-second amplitudes at HEC are correctly classified as P-waves, the event is properly classified as $M \geq 6$. In general, for vertical ground motions, misclassifying P-waves as S-waves will lead to lower magnitude estimates. However, the initially low estimates will self-correct with the S-wave arrival. Conversely, misclassifying S-waves

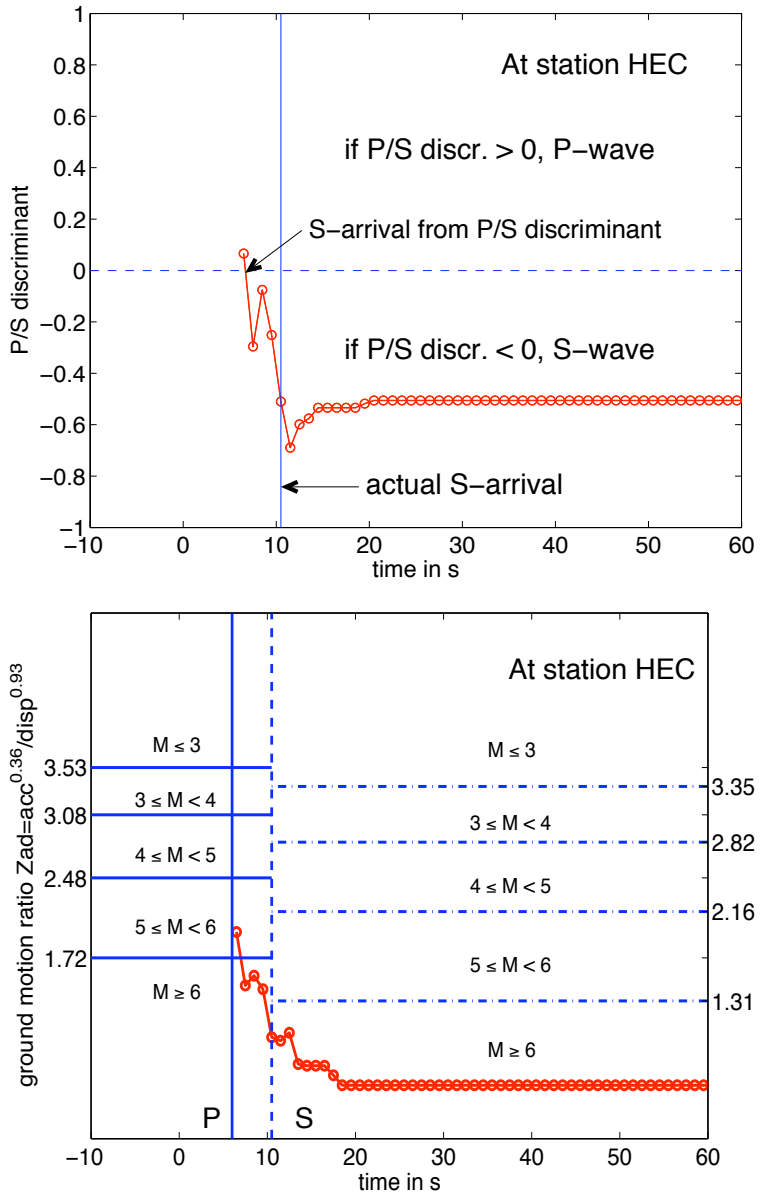

Figure 5.3: (a) The P/S discriminant, $PS = 0.43\log_{10}(Z.a) + 0.55\log_{10}(Z.v) - 0.46\log_{10}(EN.a) - 0.55\log_{10}(EN.v)$ at HEC as a function of time. The first zero crossing of PS after the P arrival is indicative of the S-arrival. The P/S discriminant does not work very well in this situation; it indicates that the S-wave arrives about 1 second after the P arrival. (b) The ground motion ratio $Z_{ad} = \frac{Z.a^{0.36}}{Z.d^{0.93}}$ as a function of time. The decision boundaries on the left-hand side are for P-waves; those on the right-hand side are for the S-wave. Even with the wrong S-arrival from the P/S discriminant, Z_{ad} is indicative of an $M \geq 6$ event 4 seconds after the initial P detection.

as P-waves leads to larger magnitude estimates.

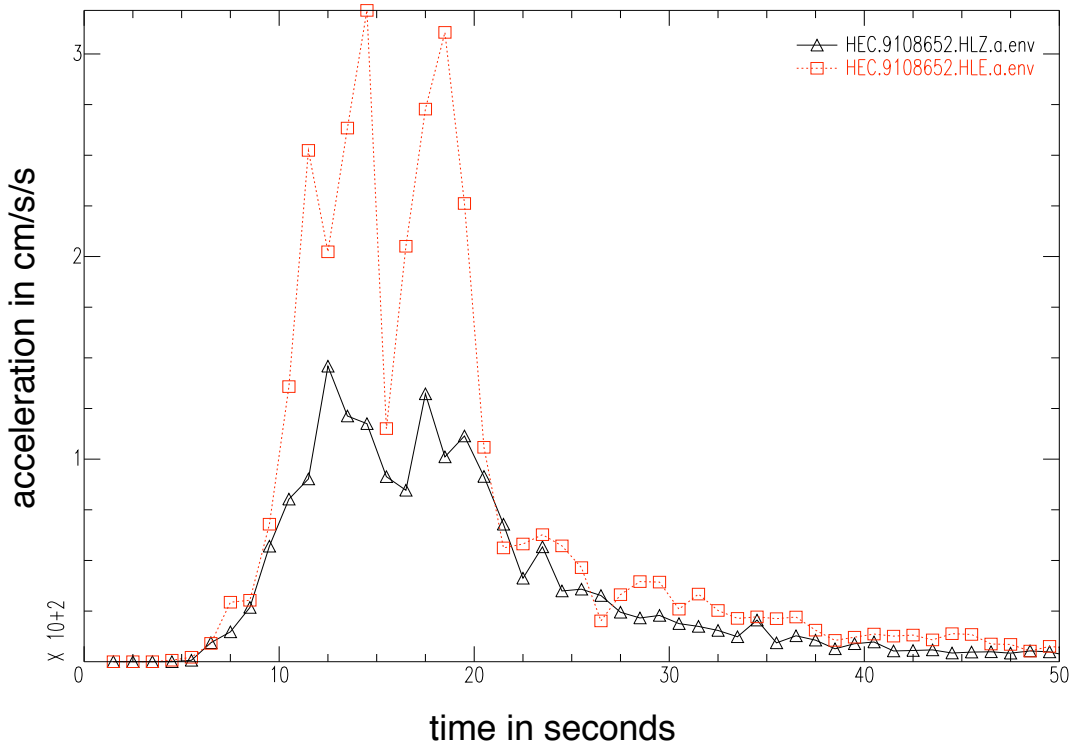

Figure 5.4: Observed vertical and horizontal acceleration envelopes at station HEC. Note that the P wave has comparable amplitudes in the vertical and horizontal directions. The P/S discriminant best works when the P-waves are strong on the vertical and relatively smaller on the horizontal, and the S-waves are strong on the horizontal and relatively smaller on the vertical.

The likelihood function described in Chapter 4 (Eqn. 4.62) allows us to combine the magnitude estimates from the vertical acceleration and displacement ground motion ratio, along with the peak available vertical velocity, and rms horizontal acceleration, velocity, and displacement amplitudes to estimate magnitude and epicentral distance. Maximizing the likelihood function yields the source estimates (in this case, magnitude M and epicentral distance R_{HEC}) that are most consistent with the available observations. Figure 5.5 shows contours of the likelihood function expressed in

terms of M and R. The likelihood is scaled to have a maximum value of 1; contours are drawn at the 0.6, 0.1, and 0.01 levels, which correspond to $\pm 1\sigma$, $\pm 2\sigma$, and $\pm 3\sigma$ about the mean of a 1-d Gaussian pdf. The "high" probability region within the 0.6 level contour is shaded. Trade-offs between M and R cannot be resolved by the 3 second observations; this is evident from the elongated contours of the likelihood function. In the absence of additional data, such trade-offs can be resolved by introducing prior information into the estimation process. Note that while trade-offs do exist, the likelihood function does have a peak. An M=6.3 event located 29 km away from HEC is the source estimate that is most consistent with the available peak amplitudes 3 seconds after the initial P detection at HEC. The Hector Mine mainshock had magnitude M=7.1 and had an epicenter 26.7 km away from HEC.

When expressing the problem in terms of magnitude and epicentral distance, the only prior information that can be included are 1) the range of epicentral distances consistent with the Voronoi cell of the first triggered station and 2) the Gutenberg-Richter magnitude-frequency relationship. If all locations within HEC's Voronoi cell are given equal weight, certain epicentral distances will have more weight. A probability density function for epicentral distances consistent with being within HEC's Voronoi cell (and thus consistent with a first P detection at HEC) can be constructed. From Figure 5.10, the P-waves have not yet arrived at the adjacent stations at the time of the initial 3 second VS estimate. This is useful information that provides additional constraints on the earthquake location.

From Rydelek and Pujol (2004) and Horiuchi et al. (2004), at t_{est}, Δt after the initial P detection, t_1, the constraint given by *not* having a P-arrival at the i^{th} station is given by

$$d_i - d_1 > \Delta t \times V \tag{5.1}$$

where V is the average P-wave velocity (about 6 km/s), and d_1 and d_1 are the epicentral distances to the first triggered and i^{th} stations. Eqn. 5.1 ignores delays due to transmission times. When t_{est} is the time of the P arrival at the i^{th} station, Eqn. 5.1 becomes an equality constraint, and the event is constrained lie along a hyperbola

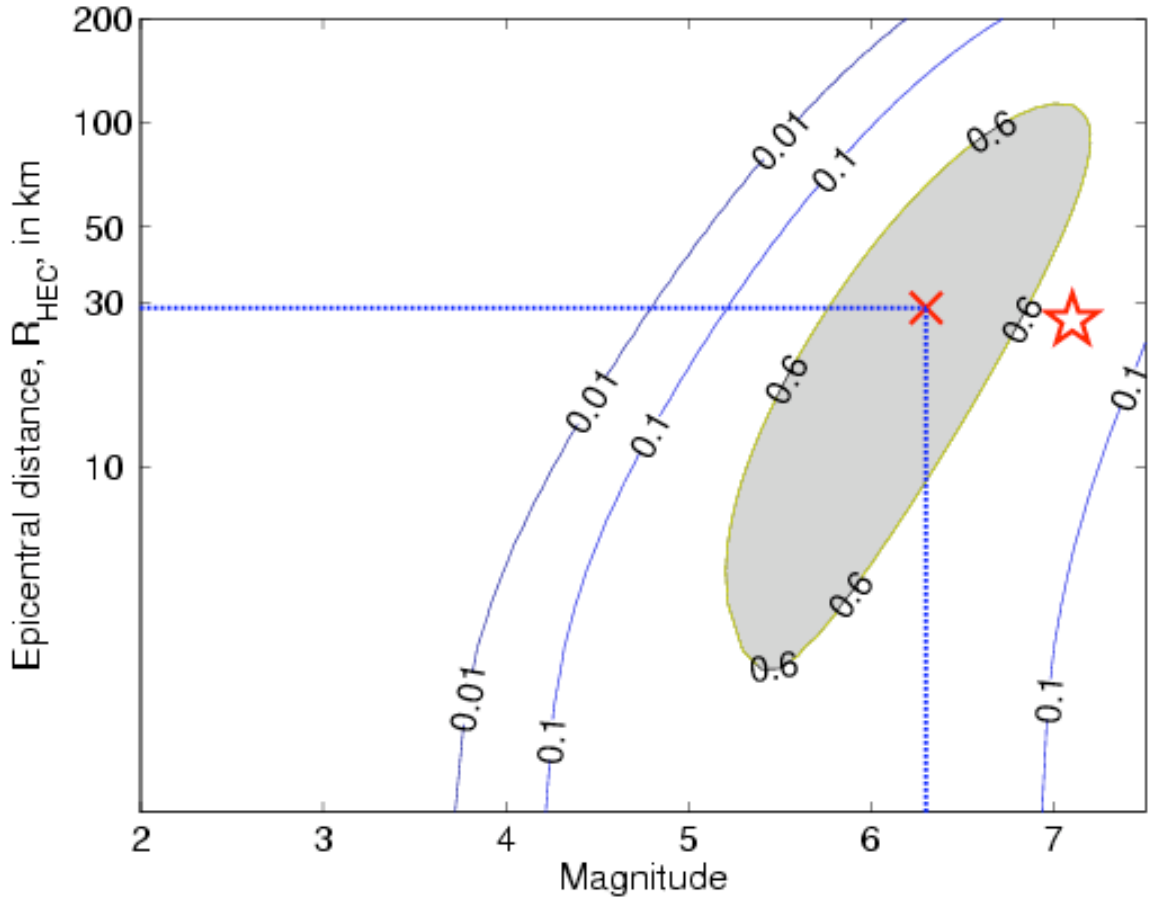

Figure 5.5: Contours of the likelihood function (expressed in terms of magnitude and epicentral distance) given the amplitudes at HEC seconds after the initial P detection. Contours are drawn at 0.6, 0.1, 0.01 levels. Regions where the likelihood function has value > 0.6 are shaded. The star marks the actual magnitude and epicentral distance to HEC (M=7.1, 26.7 km) of the Hector Mine mainshock.

between the first and i^{th} stations. In Figure 5.6, t_{est} is the time of the initial VS estimate, 3 seconds after the initial P detection. The regions consistent with the inequality constraint of Eqn. 5.1 for various stations sharing a Voronoi edge with HEC are shaded. Given the first P detection at HEC, the region of possible location is HEC's Voronoi cell. If the non-arrivals at the adjacent stations are taken into account, the region of possible location is smaller (shaded region in Figure 5.7). In Figure 5.8, the solid line (black) shows the pdf of epicentral distances (scaled to a maximum value of 1) consistent with a first arrival at station HEC. The dashed line shows the pdf when accounting for the non-arrivals at the adjacent stations 3 seconds after the initial P detection.

At the time of the initial VS estimate, the available amplitudes (and arrivals) are not able to fully resolve the trade-offs between magnitude and distance, as evidenced by the elongated contours of the likelihood function in Figure 5.5. The shape of the Bayes posterior density function, whose maxima correspond to the VS estimates, will depend on the form of the prior. From Figure 5.8, whether or not the (non-) arrivals at the surrounding stations is taken into account has some minor effects on the details of the epicentral distance pdf. The effect on the Bayes posterior of taking into account this inter-arrival time, or time between subsequent P arrivals, is also minor. Whether or not to use the Gutenberg-Richter magnitude-frequency relationship in the prior makes a more considerable difference. This is illustrated in Figure 5.9. The Gutenberg-Richter (G-R) relationship states that smaller earthquakes occur more frequently than larger events. Thus, the trade-offs in the likelihood function (Figure 5.5) are resolved in favor of smaller magnitude events at closer distances to the station. Without the G-R in the prior, the VS estimate is an M=6.2 event located about 30 km away from the station. With the G-R in the prior, the VS estimate is an M=5.2 event located about 15 km from the station.

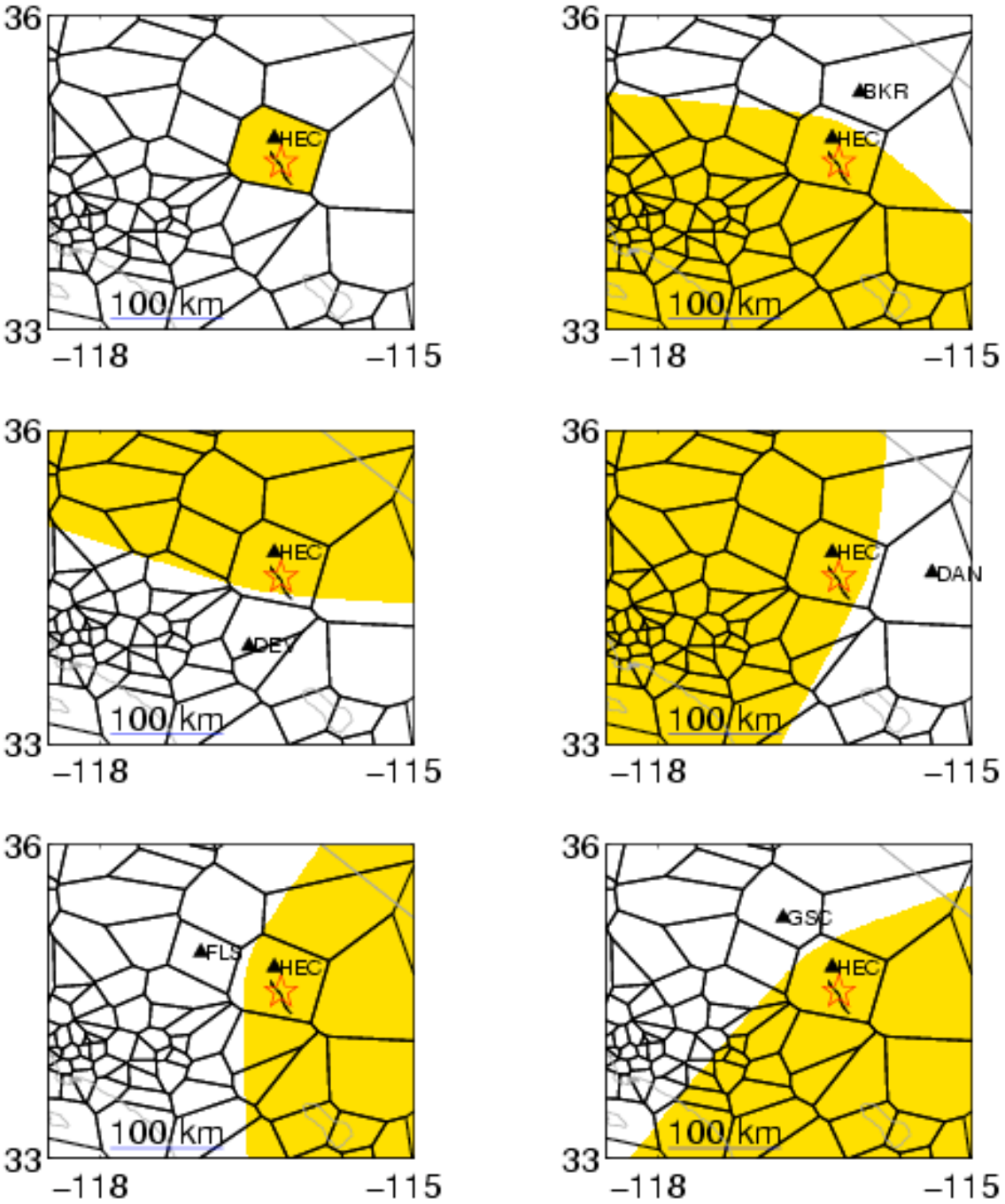

Figure 5.6: The shaded regions are those consistent with (a) the first P detection at HEC, and (b-f) no P arrivals at BKR, DEV, DAN, FLS, and GSC (they share Voronoi edges with HEC) at the time of the first VS estimate, 3 seconds after the initial P detection. Other stations sharing Voronoi edges with HEC (not shown, but providing similar constraints) are VTV, SBPX, and SVD.

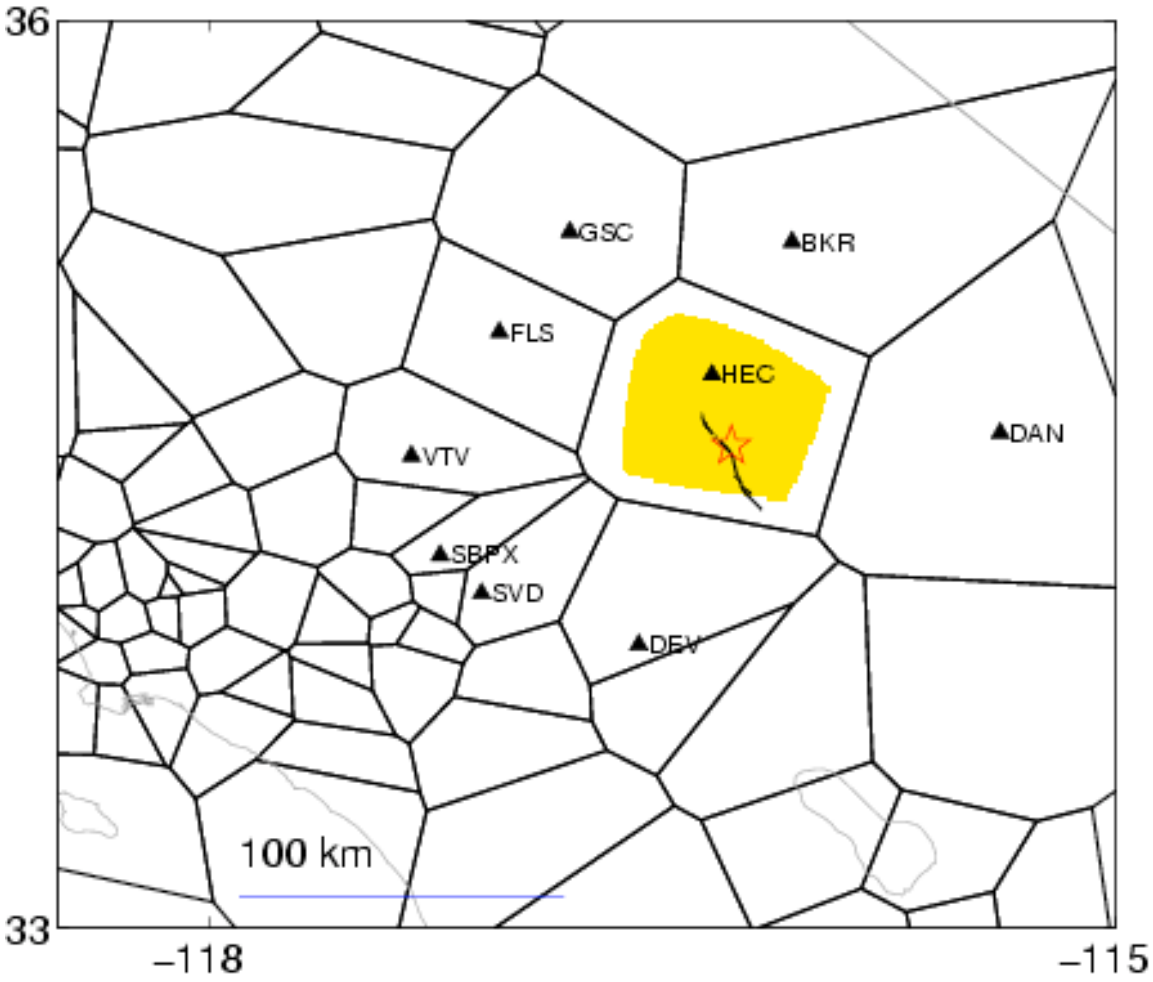

Figure 5.7: The region of possible location as constrained by P-wave arrival and non-arrival information from the first triggered station, HEC, and stations sharing a Voronoi edge: BKR, DEV, DAN, FLS, GSC, SVD, VTV, and SBPX.

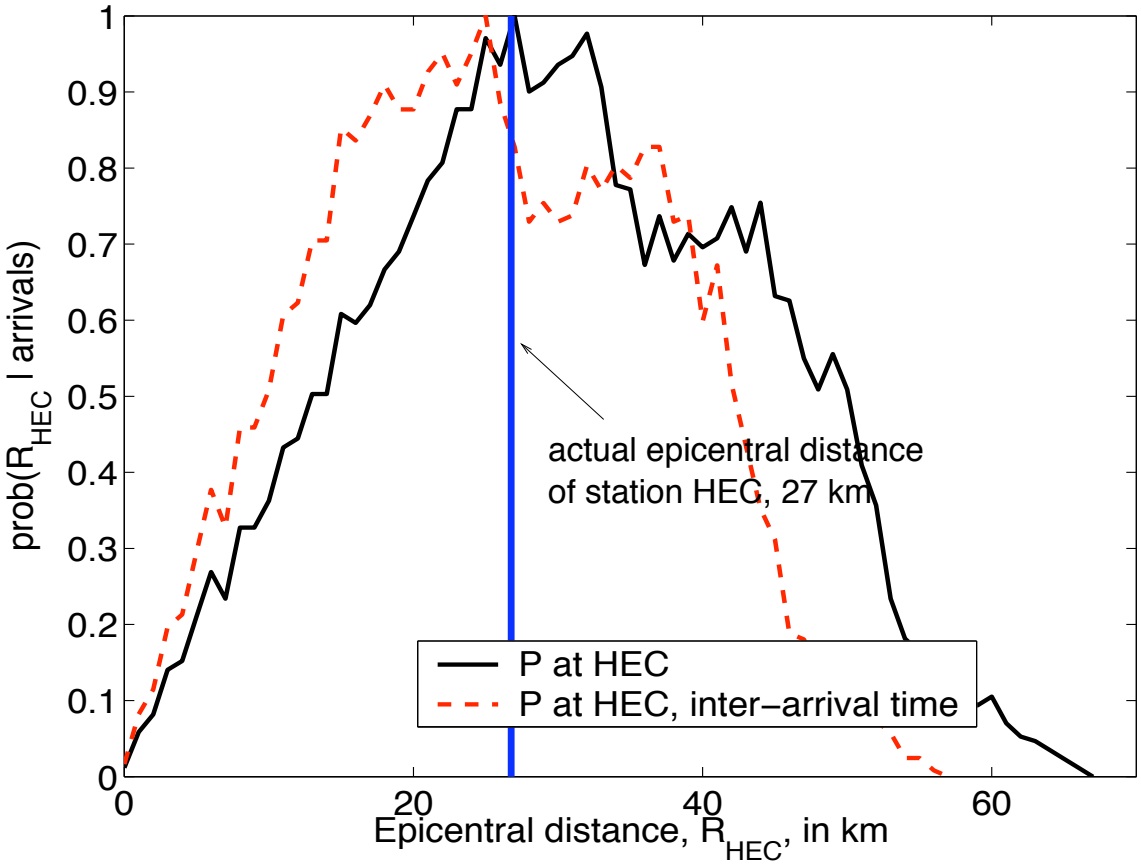

Figure 5.8: The range of possible epicentral distances R_{HEC} taking into account 1) the initial P detection at HEC (solid black line), 2) there are no other arrivals at adjacent stations 3 seconds after the initial P detection (red dashed line).

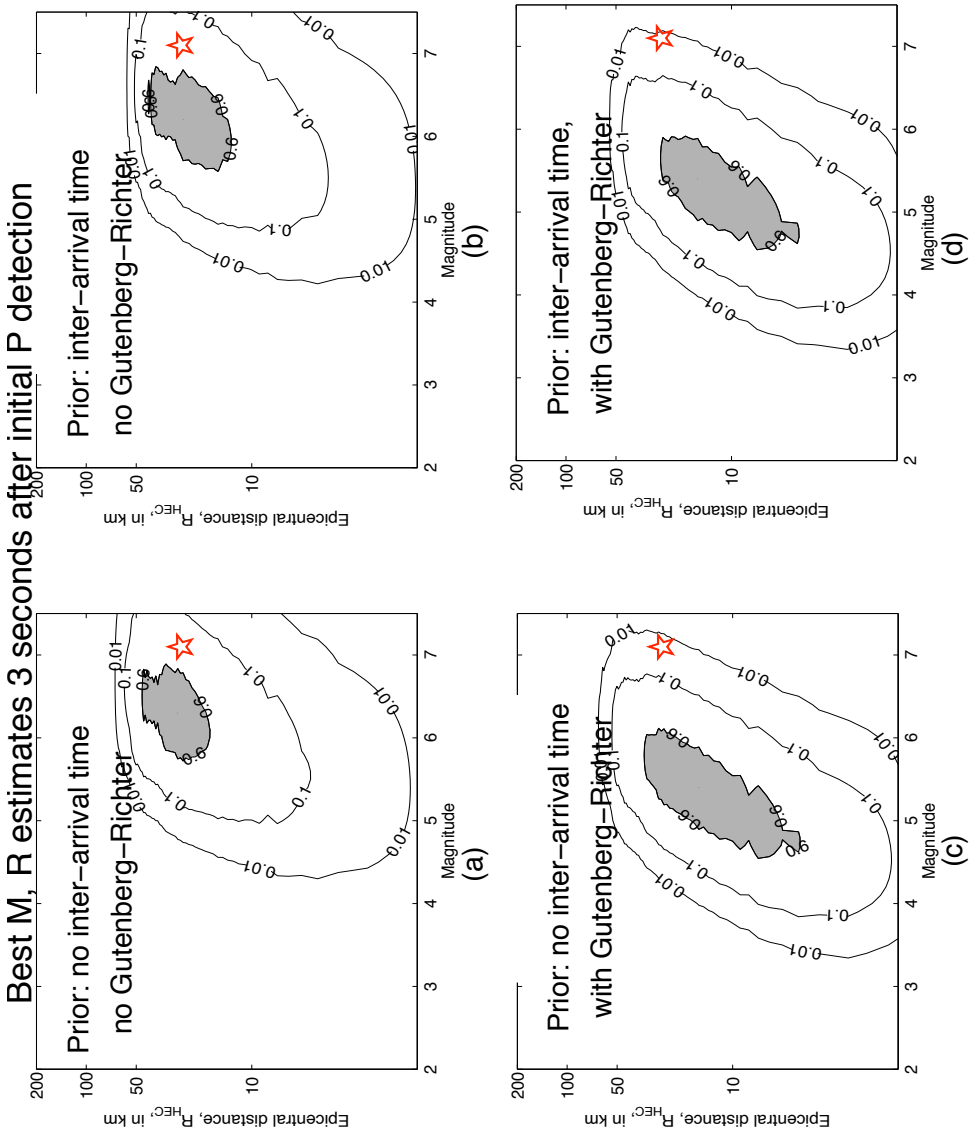

Figure 5.9: Including the Gutenberg-Richter magnitude-frequency relationship and the information that are no P arrivals at the stations adjacent to HEC 3 seconds after the initial P detection at HEC affects the shape of the Bayes posterior, and hence the VS estimates, 3 seconds after the initial P detection at PKD. Regions in M-R space where $prob(M, R|data) \geq 0.6$ are shaded. The VS estimates for each of the different combinations of prior information are the centers of the shaded regions. Using the Gutenberg-Richter relationship favors smaller magnitude events located at closer distances to the station.

5.4 Multiple station estimates: solving for magnitude and epicentral location

Updating the VS estimates as the ground motions propagate to further stations is more convenient when the problem is expressed in terms of magnitude and epicentral location (latitude and longitude). This change in coordinate system also allows information about fault locations and previously observed seismicity to be included in the Bayes prior.

Figure 5.10 shows the contours of the P-wave wavefront at the times of various VS estimates- at 3, 5.5, 7, 8, 14, 34, and 74 seconds after the initial P detection (add 6 seconds to get VS estimate times relative to the earthquake origin time).

From Figure 5.10, at 13 seconds after the origin time (or 7 seconds after the initial P detection), the P waves have not yet arrived at stations adjacent to HEC. Thus, the first 3 VS estimates, at 9, 11.5, and 13 seconds after the origin time (or 3, 5.5, and 7 seconds after the initial P detection) involve only the observed amplitudes at a single station. As previously discussed, the lack of P-arrivals at the adjacent stations is valuable information that serves to constrain the possible location. The Bayes prior strongly influences these early VS estimates, when there is insufficient amplitude and arrival information to uniquely determine the magnitude and epicentral location. In this example, the Bayes prior includes information regarding the station geometry, previously observed seismicity, and the Gutenberg-Richter magnitude-frequency relationship. Fault locations are not included. Previous to the Hector Mine mainshock, the Lavic Lake fault on which the rupture initiated was not considered an active fault (http://pasadena.wr.usgs.gov/hector/report.html, 1999). The methods to include seismicity and fault information used are somewhat ad hoc. The seismicity prior was generated by assigning locations within a 5 km radius of an earthquake in the 24 hours preceding the mainshock a particular weight. This weight was chosen to be 1.3; the combined effect of the 18 events in the foreshock sequence weights the area around this cluster 30 times more than other locations. A scaling factor is introduced such that the seismicity prior integrates to 1 over the latitude and longitude range

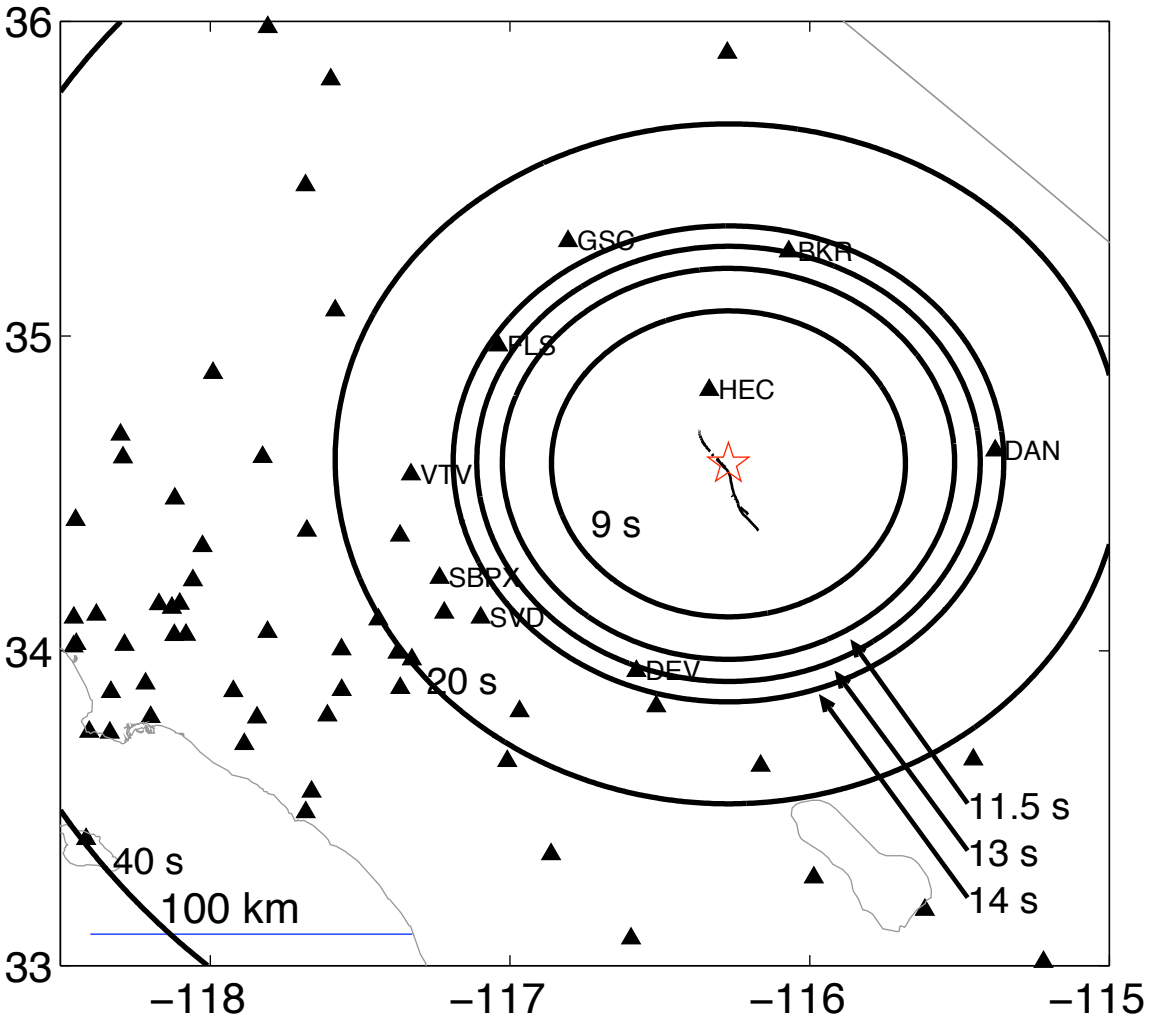

Figure 5.10: SCSN stations used to update the VS estimates for the 1999 M=7.1 Hector Mine mainshock. Contours show the P-wave wavefront (for a point source at the epicenter) at the times of the VS estimates at t=3, 5.5, 7, 8, 14, 34, and 74 seconds after the initial P detection; add 6 seconds to get the estimate times relative to the earthquake origin time, as labeled in Figure. The 74 second contour is beyond the boundaries of the plot.

considered. For simplicity, the seismicity prior is independent of magnitude. That is, the 5 km radius surrounding an M=4 event receives equal weight as the region surrounding an M=1.5 event. A short-term seismicity-based earthquake forecast, such as STEP by Gerstenberger et al. (2003), would be the "proper" way to include the effects of previous seismic activity on current levels of earthquake hazard. Presumably, a formal method would be able to properly account for the effects of the 1992 M=7.3 Landers earthquake, as well as the foreshock sequence that immediately preceded the Hector Mine mainshock.

The station geometry prior is generated by calculating the nearest neighbor regions of the operating stations. Locations within the first triggered station's Voronoi cell are assigned a weight of 100; all other locations are assigned a weight of 1. A scaling factor is introduced such that the station geometry prior integrates to 1 over the latitude and longitude range considered. The location prior $prob(lat, lon)$ is obtained by multiplying the seismicity and station geometry priors.

The various updates to the VS estimates are calculated with and without the Gutenberg-Richter relationship. When the Gutenberg-Richter relationship is used, the magnitude prior has the form $prob(M) = 10^{1-M}$; when it is not included, the magnitude prior is $prob(M) = k$, where k is a constant. The magnitude prior is scaled so that it integrates to 1 over the magnitude range considered ($2 \leq M \leq 7.5$). The Bayes prior is the product of the magnitude and location priors. That is, $prob(M, lat, lon) = prob(M) \times prob(lat, lon)$. Again, it is a simplifying assumption to treat the magnitude and location information as independent. Ideally, some type of short-term earthquake forecast, such as STEP or ETAS, that accounts for the magnitudes of the previously observed earthquakes and scales the problem such that it is consistent with the total number of earthquakes predicted by long-term forecasts, should be used to generate the Bayes prior.

Given only the peak amplitudes at HEC 3 seconds after the initial P detection (no prior information), Figure 5.11 shows the locations consistent with 6 different magnitude ranges: $2 \leq M < 3$, $3 \leq M < 4$, $4 \leq M < 5$, $5 \leq M < 6$, $6 \leq M < 7$, and $M \geq 7$. For each magnitude range, the contours of the location marginal of

the likelihood function (integrated over the given magnitude range and scaled to a maximum value of 1) are drawn at the 0.01, 0.1, and 0.6 levels. The regions where $prob(lat, lon|data) \geq 0.6$ are shaded. In general, the area consistent with larger magnitudes is much larger than the regions consistent with smaller magnitudes.

The VS estimate for magnitude and epicentral location 3 seconds after the initial P detection is a combination of the Bayes prior, the likelihood function given the available amplitudes (Figure 5.11), as well as the constraints on earthquake location given the available P arrivals and non-arrivals.

In the following figures showing the VS location estimates, the color scales with the probability of the event being located at a given location and the contours convey the magnitude estimates without the Gutenberg-Richter magnitude-frequency relationship. For comparison, the star marks the epicentral location reported by SCSN. With the sequence of 18 events within 1 km of the epicentral region in the 24 hours preceding the manishock, the initial VS location estimate is an $M = 6.2 \pm 0.495$ event within 2 km of the actual epicenter with only a single P arrival and 3 seconds of observed amplitudes at HEC. This is shown in Figure 5.12. The region of probable location is peaked about the foreshock cluster, and is smaller than the Voronoi cell of HEC. The boundaries of the region where $prob(lat, lon|data) > 0$ are determined by the information that there are no other P-arrivals at the stations sharing Voronoi edges with HEC. The unshaded regions in Figure 5.12 are not consistent with an initial P arrival at HEC and no subsequent P arrivals at other stations 3 seconds later. The longer the interval between the first and subsequent P arrivals, the more the region of probable location contracts towards HEC. There are no subsequent arrivals at the time of the second and third VS updates at 5.5 and 7 seconds after the initial P detection. However, the non-arrival information provides evolving constraints on the possible locations.

By 8 seconds after the initial P detection, the P waves arrive at stations BKR and DEV. With 3 arrivals, the earthquake location is uniquely determined. However, the magnitude estimates continue to evolve. The VS magnitude estimate 8 seconds after the initial detection (14 seconds after earthquake origin time) is $M = 7.2 \pm 0.289$

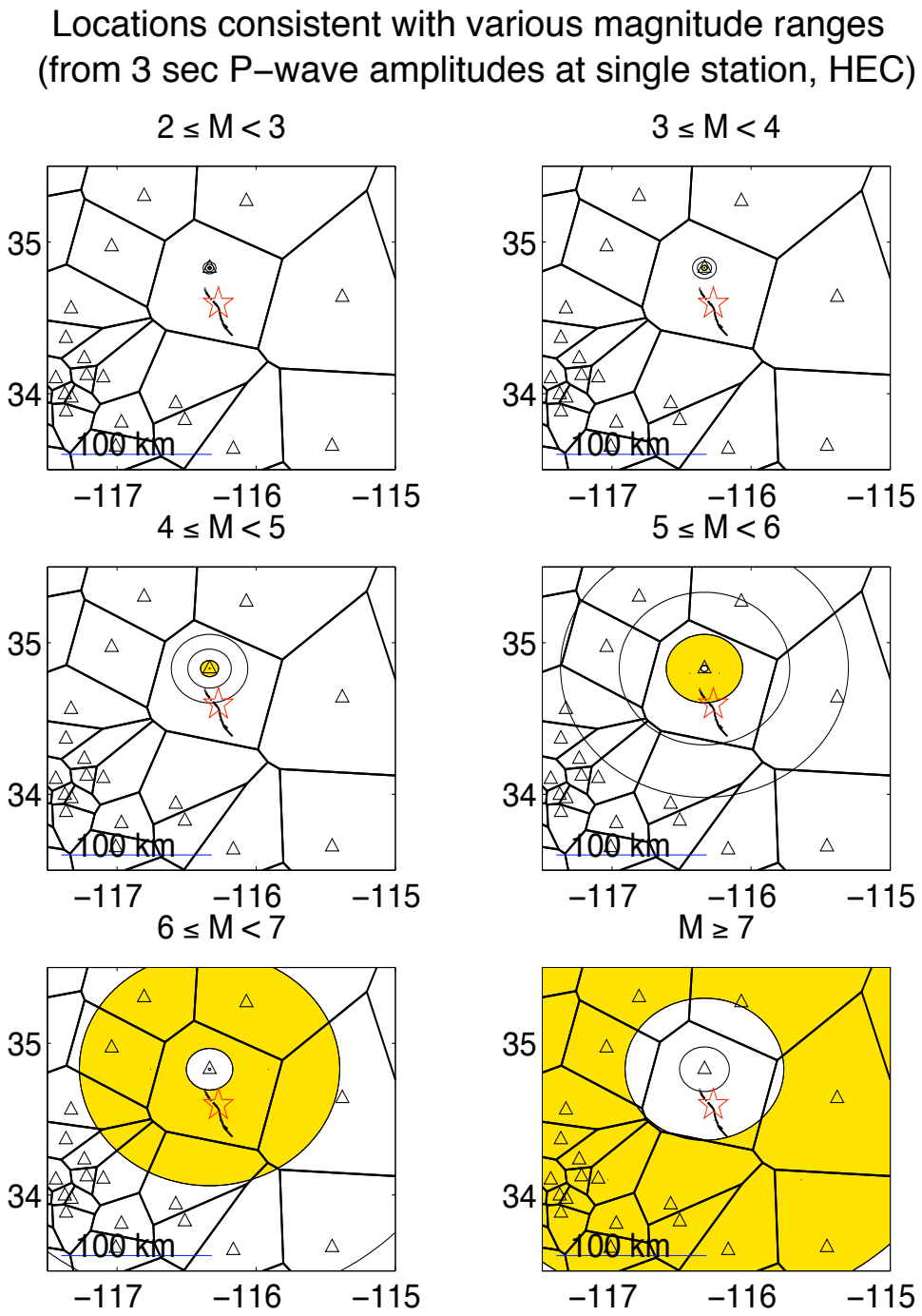

Figure 5.11: The shaded regions in each subplot are the locations consistent with the given magnitude range using the peak P-wave amplitudes 3 seconds after the initial P detection at HEC (no prior information included). Note that the total area of the shaded "high probability" regions is much larger for events with $M \geq 5$ than for smaller magnitudes. 3 seconds of P-wave amplitudes from the first triggered station cannot uniquely resolve magnitude and location (although this information is enough to broadly estimate the probable magnitude range). The trade-offs shown here are comparable to those shown in Figure 5.5.

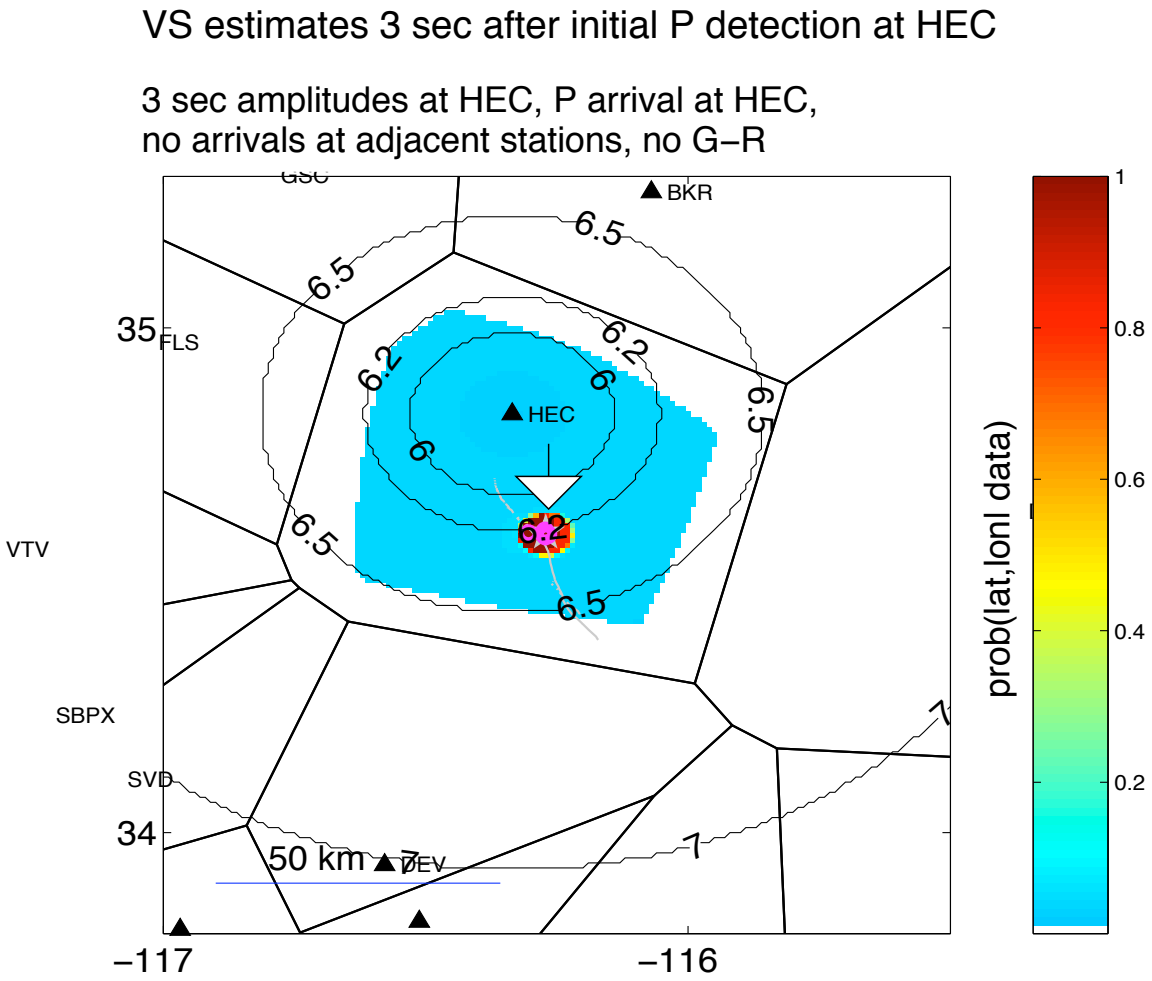

Figure 5.12: The colors scale with the probability that the earthquake is at a given location. The contours are the magnitude estimates *without* the Gutenberg-Richter relationship in the Bayes prior. The initial VS estimate locates the on-going event within the concentrated cluster of 18 $M \geq 1.5$ events which occurred in the 24 hours preceding the mainshock. The magnitude estimate *without* G-R is $M = 6.2 \pm 0.495$; *with* G-R, it is $M = 5.7 \pm 0.52$. The shape of the blue shaded region within HEC's Voronoi cell is governed by the information that there are no P arrivals at adjacent station 3 seconds after the initial P detection at HEC. The star marks the epicenter location as reported by CISN.

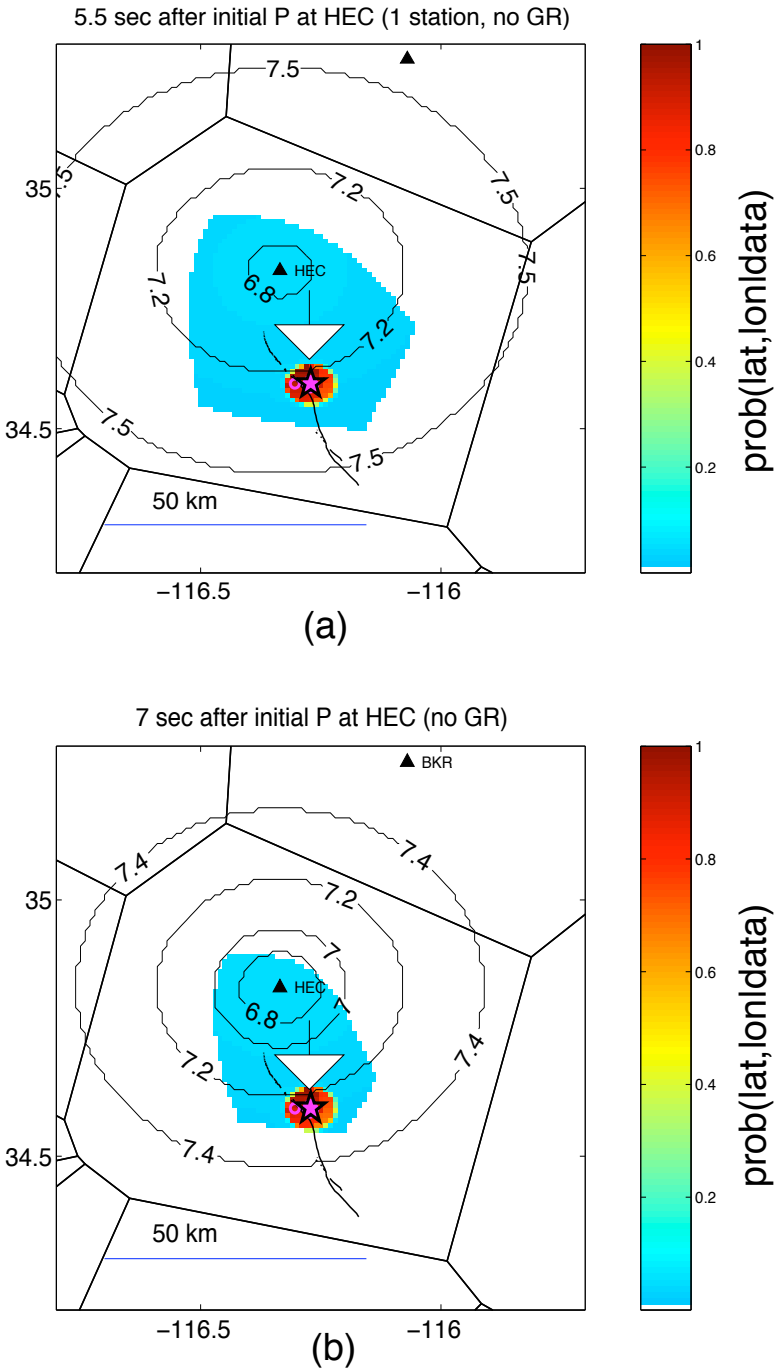

Figure 5.13: The VS estimates at 5.5 (a) and 7 (b) seconds after the initial P detection. The VS location estimate is in the region of the foreshock cluster. The difference in the shaded regions in (a) and (b) is due to the length of time without P arrivals at stations adjacent to HEC. The VS magnitude estimate at 5.5 sec after the initial detection is $M = 7.2 \pm 0.415$ without the G-R and $M = 6.6 \pm 0.55$ with the G-R. The VS magnitude estimate at 7 sec after the initial detection is $M = 7.1 \pm 0.327$ without the G-R and $M = 6.9 \pm 0.409$ with the G-R. The 7 sec VS magnitude estimates include S-wave amplitudes at HEC.

without G-R and $M = 7.0 \pm 0.215$ with G-R. This estimate is based on the peak P- and S-wave amplitudes at HEC. (The amplitudes at other stations will only be included once there is more than 3 seconds of data after the P detection at a given station.)

Figure 5.15 shows the availability of amplitude and arrival observations as a function of time. For seismic early warning, the earlier estimates are the most important. There is typically not much data in the first few seconds after the initial P detection. This is when the prior information is most useful. The prior information included in the Bayes prior includes station geometry and previously observed seismicity. The uncertainty in the VS estimates decreases as $\frac{1}{\sqrt{N}}$ (since observations are assumed independent), where N is the number of stations contributing data. Figure 5.15 shows the magnitude estimates as a function of time. The uncertainties are initially large, and decrease like $\frac{1}{\sqrt{N}}$. The VS estimates including the Gutenberg-Richter relationship in the Bayes prior is slower to approach the CISN-reported magnitude than the other estimates. Figure 5.17 shows the evolution of the VS location estimates as a function of time. The VS location estimates are always within 5 km of the mainshock epicenter, even with only the first P arrival at HEC; the foreshock sequence provides very strong and relevant prior information.

The VS estimates at 80 seconds after the origin time (or 74 seconds after the initial P detection) are not useful for seismic early warning, since the large ground motions have, by now, propagated to the areas that would have had strong shaking (see Figure 5.10). However, the VS estimates (using a uniform prior) at large times after the earthquake origin time provide very robust amplitude-based location estimates. These amplitude-based locations are comparable to the strong motion centroid of Kanamori (1993). Figure 5.18 shows that the SCSN-reported, arrival-based location (star) is consistent with the VS amplitude-based estimate (green contours). Recall that amplitude- and arrival-based location methods are relatively independent, since they use different types of information. When there is agreement between these two independent estimates, then the arrival-based location is most likely to be correct. Another arrival-based location (blue contours) obtained by minimizing the residual

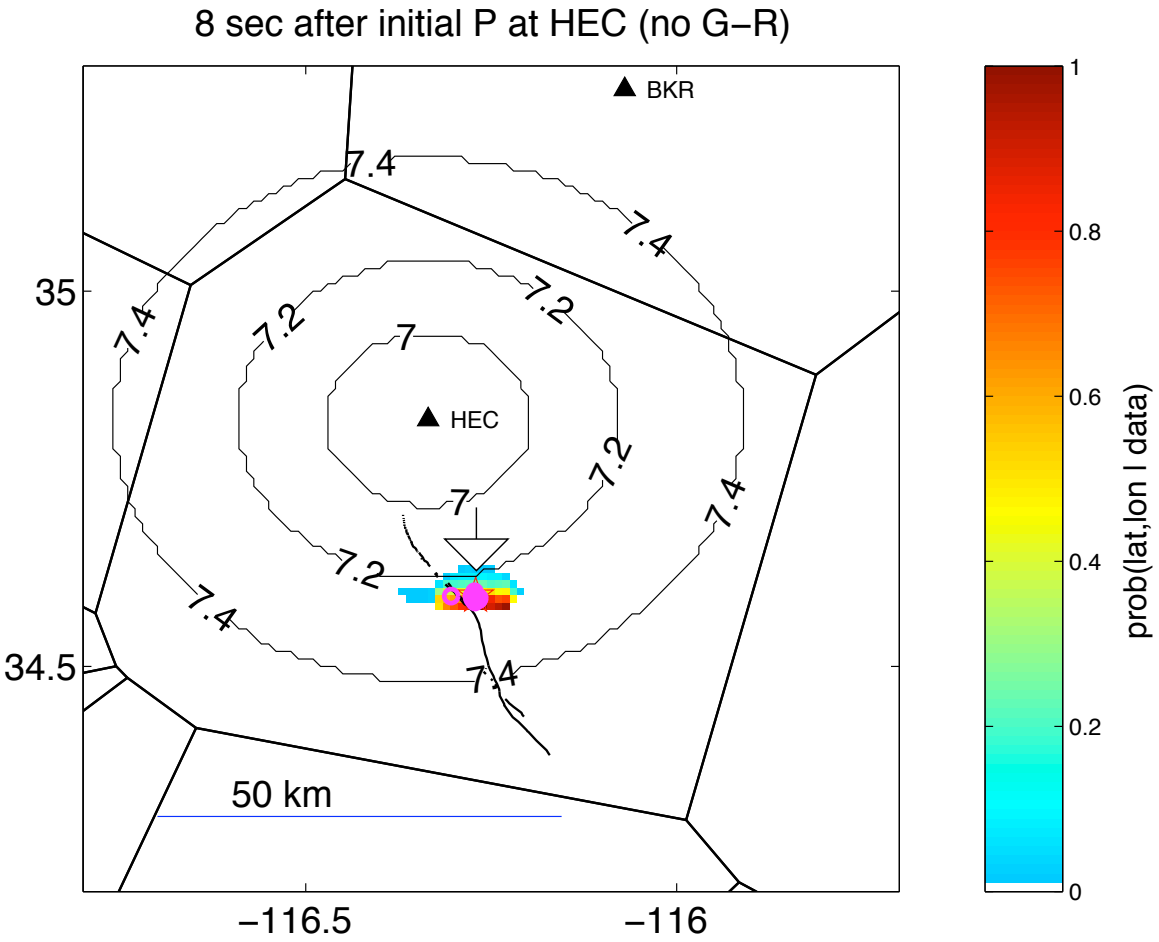

Figure 5.14: The VS estimate at 8 seconds after the initial P detection. By this time, second and third P arrivals at BKR and DEV uniquely determine an epicentral location. Even without the second and third arrivals, the VS location estimate was always within 5 km of the epicentral location due to the peak in the seismicity prior from the foreshock cluster. The VS magnitude estimate without G-R is $M = 7.2 \pm 0.289$, with G-R is $M = 7.0 \pm 0.215$. The magnitude estimate is based on P- and S-wave amplitudes at HEC. BKR and DEV do not contribute amplitude information until there is more than 3 seconds of data after the P detection at that station.

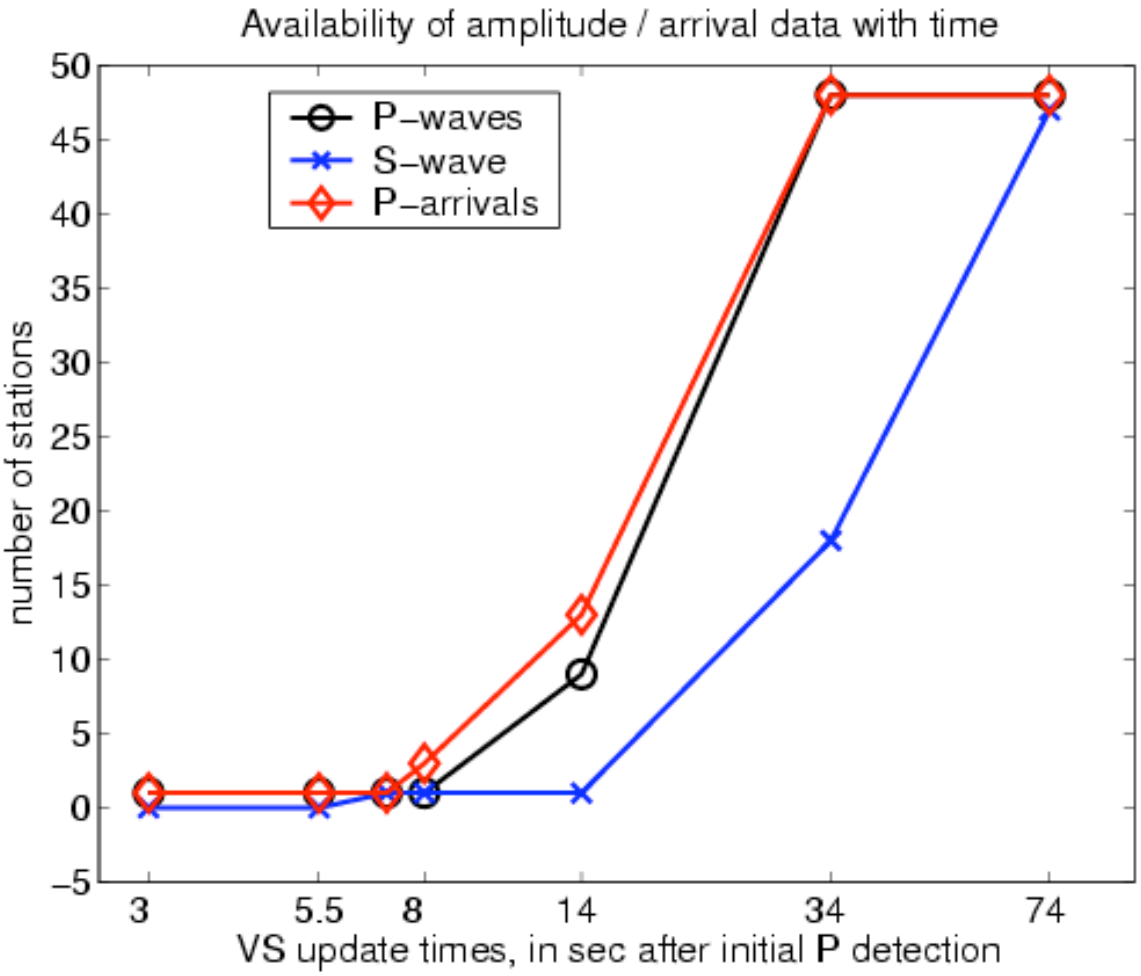

Figure 5.15: The number of stations contributing P-wave arrivals and peak P- and S-wave amplitudes to the VS estimates as a function of time. The foreshock sequence of 18 events in the 24 hours preceding the mainshock within 1 km of the mainshock epicentral region provides very strong prior information.

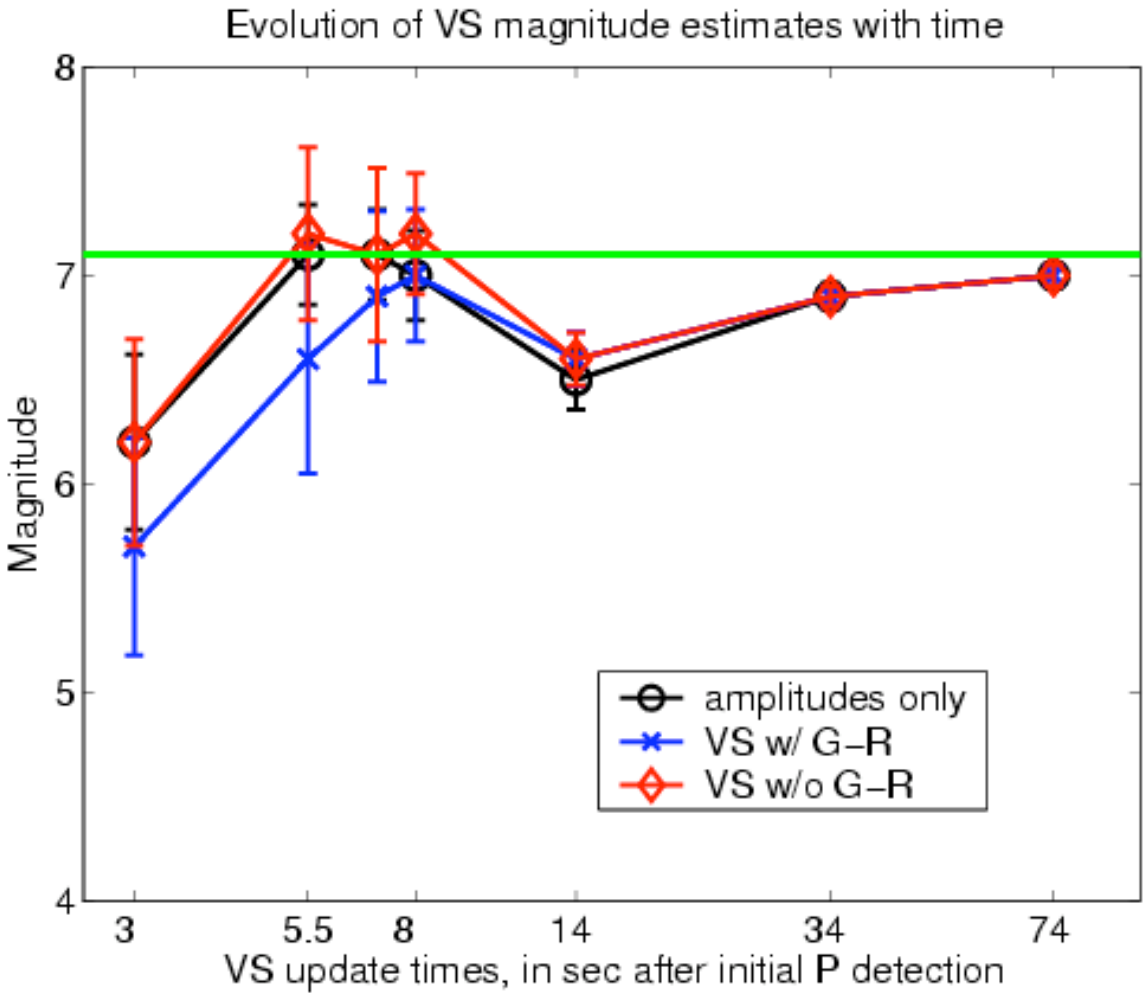

Figure 5.16: The evolution of various magnitude estimates as a function of time. The estimates labeled "amplitude only" do not use prior information. The VS magnitude estimates with and without the Gutenberg-Richter relationship in the Bayes prior are shown. The horizontal line denotes the SCSN magnitude of M=7.1. The VS estimates without the G-R approach the SCSN magnitude faster than those which include the G-R in the Bayes prior.

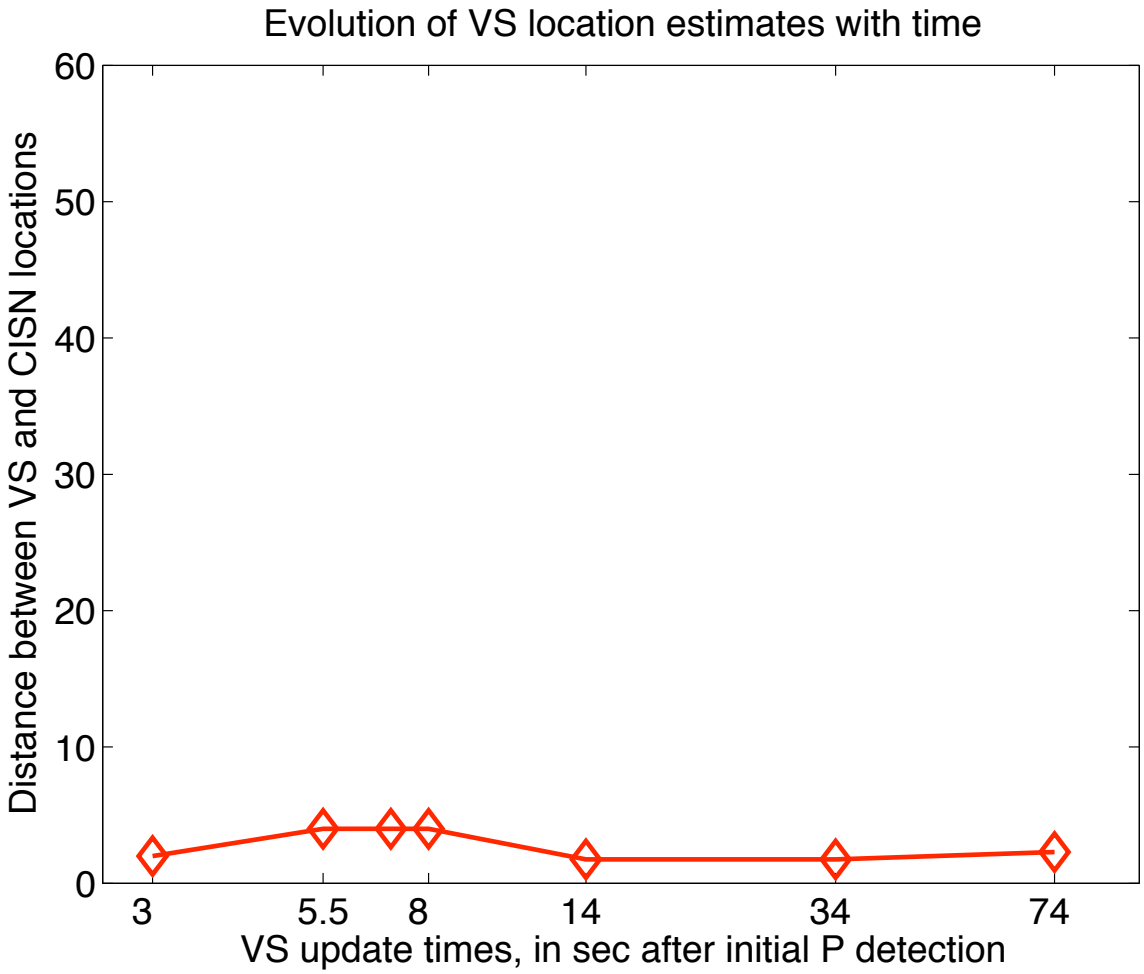

Figure 5.17: The evolution of the VS location estimates as a function of time. The distance between the VS location estimate and the SCSN-reported location is shown. The SCSN location is typically based on numerous arrivals and waveforms. The VS estimates are based on the available amplitudes and arrival information as shown in Figure 5.15. The 18 events in the foreshock sequence that occurred in the 24 hours preceding the mainshock provides very strong and relevant prior information. The VS location estimate, even at 3 seconds after the initial P detection, with a single P arrival and amplitudes from a single station, is always within 5 km of the mainshock epicenter.

between predicted and observed P arrival times from 48 stations is shown. While it does not precisely match the SCSN-location, it is consistent with the amplitude-based estimate.

Figure 5.19 compares the magnitude estimates from the vertical ground motion ratios alone at (a) 14 and (b) 74 seconds after the initial P detection. From the 14 second ground motion ratios, it appears that the ratio-based magnitude estimates are distant-dependent. However, from the 74 second ground motion ratios, there is no apparent distance-dependence. The ratio-based magnitude estimates are relatively independent of distance, but are do vary with time until the peak vertical ground motions arrive at the stations. This was shown for station HEC in Figure 5.3, and may explain the dip in the magnitude estimate versus time plot shown in Figure 5.16. The peak observed P- and S-wave amplitudes are compared with the expected P- and S-wave ground motion levels given by the attenuation relationships discussed in Chapter 2 in Figures 5.20 and 5.21. There is a relatively good agreement between the observed and expected ground motion levels. This is expected, since the Hector Mine dataset was used to develop the envelope attenuation relationships.

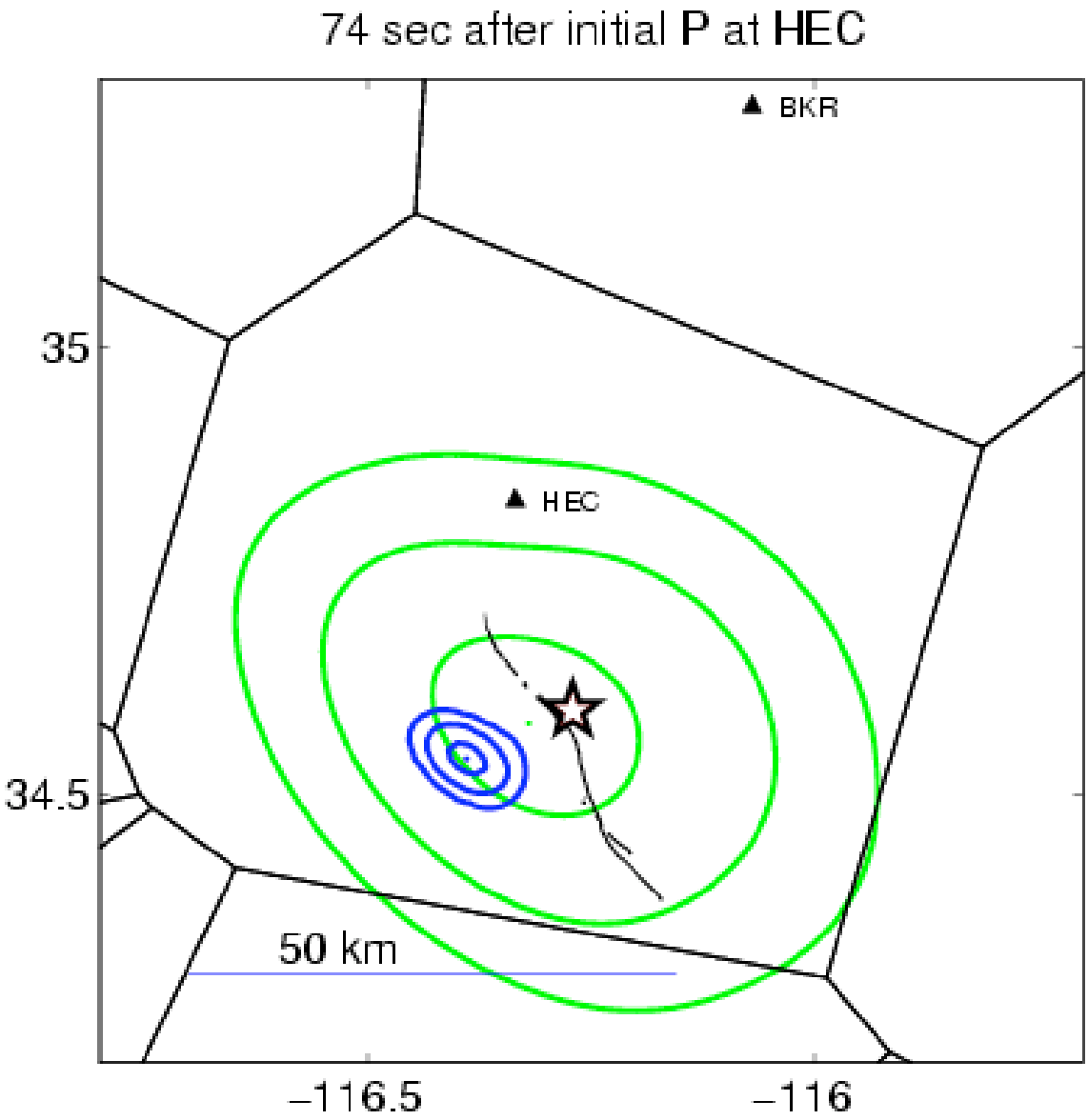

Figure 5.18: Comparison of amplitude- and arrival-based location estimates 74 seconds after the initial P detection. The amplitude-based locations (green contours) are derived from the distribution of peak P- and S-wave amplitudes from 48 stations. The arrival-based location (blue contours) is derived from 31 P-wave arrivals. The arrival-based location in this analysis should match the SCSN-reported location, which is marked by a star. In general, the amplitude-based locations are consistent with the arrival-based locations (the green contours contain the blue contours and the star). Recall that these 2 different location estimates are relatively independent, since they involve different observed quantities.

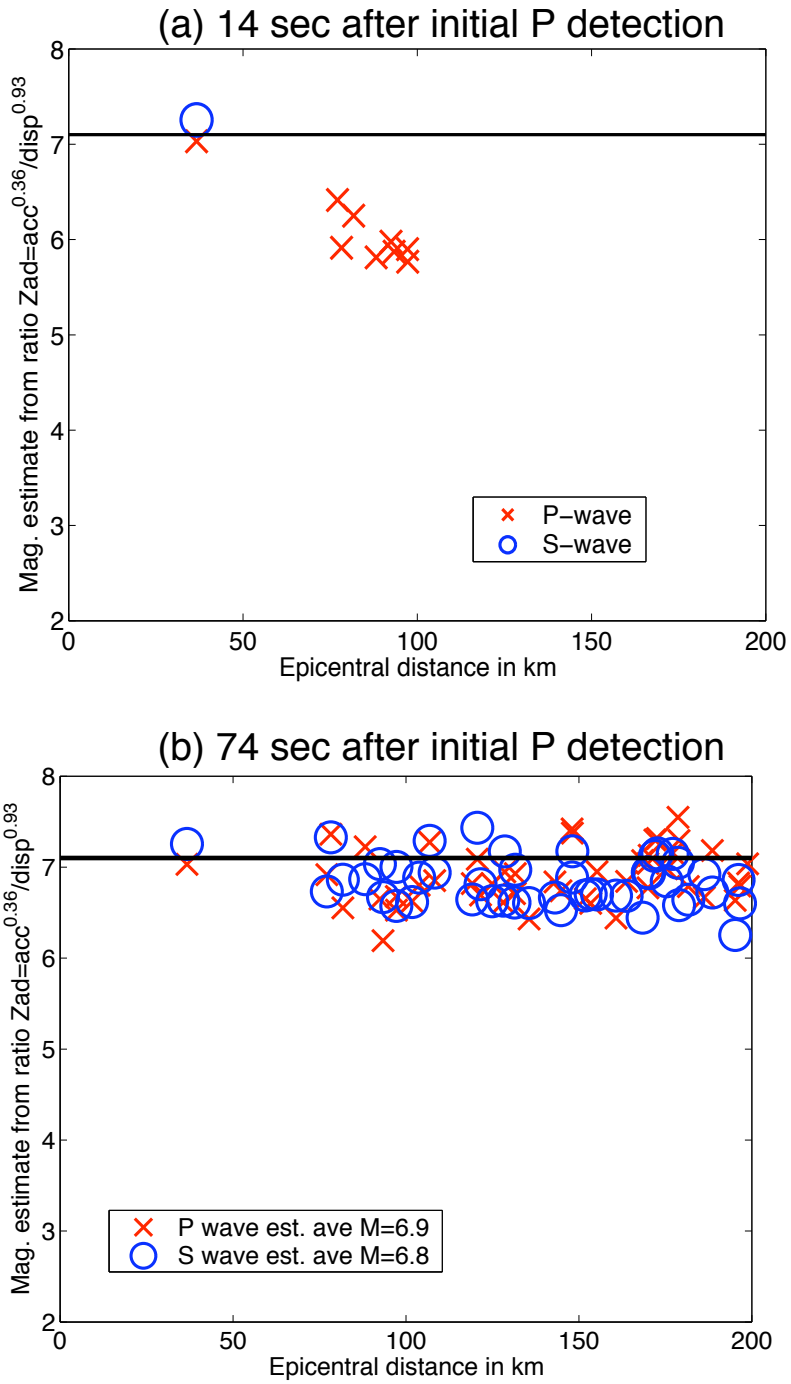

Figure 5.19: Magnitude estimates based on the vertical ground motion ratio, $Zad = acc^{0.36}/disp^{0.93}$, for P- and S-waves as a function of distance at (a) 14 and (b) 74 seconds after the initial P detection. From (b), the ratio-based magnitude estimates are relatively independent of distance. However, from comparing (a) and (b), there is a time-dependence to these ratio-based magnitude estimates. This time-dependence can also be seen in Figure 5.3.

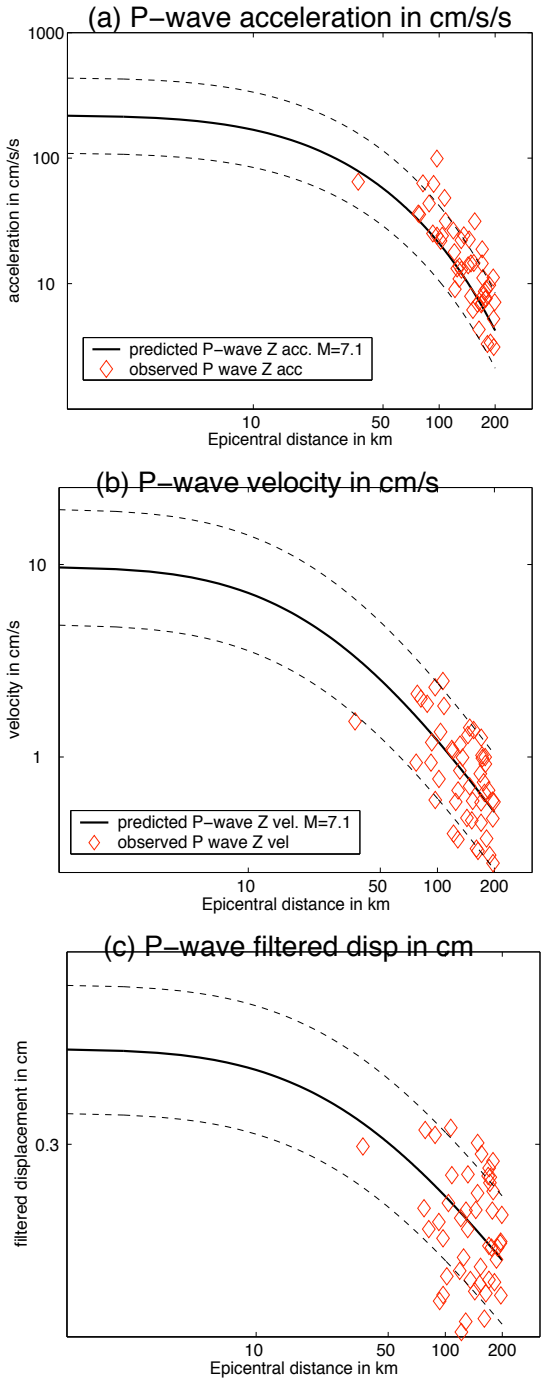

Figure 5.20: The predicted ground motion levels as a function of epicentral distance given by the vertical P-wave envelope attenuation relationships discussed in Chapter 2 for an M=7.1 earthquake and the observed peak vertical P-wave (a) acceleration, (b) velocity, and (c) filtered displacement amplitudes from the M=7.1 Hector Mine mainshock.

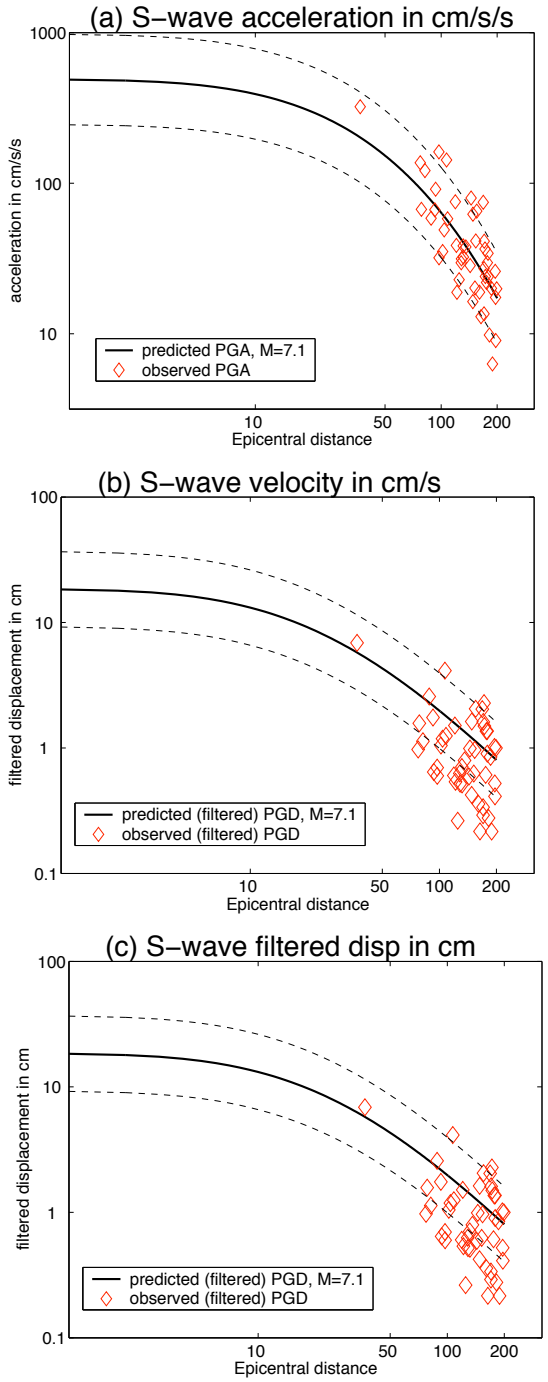

Figure 5.21: The predicted ground motion levels as a function of epicentral distance given by the rms horizontal S-wave envelope attenuation relationships discussed in Chapter2 for an M=7.1 earthquake and the observed peak rms horizontal S-wave (a) acceleration, (b) velocity, and (c) filtered displacement amplitudes from the M=7.1 Hector Mine mainshock.